

# The 2dF-SDSS LRG and QSO survey: Evolution of the Luminosity Function of Luminous Red Galaxies to $z = 0.6$

David A. Wake<sup>1,2</sup>, Robert C. Nichol<sup>1</sup>, Daniel J. Eisenstein<sup>3</sup>, Jon Loveday<sup>4</sup>, Alastair C. Edge<sup>2</sup>, Russell Cannon<sup>5</sup>, Ian Smail<sup>6</sup>, Donald P. Schneider<sup>7</sup>, Ryan Scranton<sup>15</sup>, Daniel Carson<sup>1</sup>, Nicholas P. Ross<sup>2</sup>, Robert J. Brunner<sup>8</sup>, Matthew Colless<sup>5</sup>, Warwick J. Couch<sup>9</sup>, Scott M. Croom<sup>5</sup>, Simon P. Driver<sup>10</sup>, José da Ângela<sup>2</sup>, Sebastian Jester<sup>14</sup>, Roberto de Propriis<sup>11</sup>, Michael J. Drinkwater<sup>12</sup>, Joss Bland-Hawthorn<sup>5</sup>, Kevin A. Pimbblet<sup>12</sup>, Isaac G. Roseboom<sup>12</sup>, Tom Shanks<sup>2</sup>, Robert G. Sharp<sup>5</sup>, Jon Brinkmann<sup>13</sup>

<sup>1</sup>*Institute of Cosmology and Gravitation (ICG), Mercantile House, University of Portsmouth, Portsmouth, PO1 2EG, UK*

<sup>2</sup>*Dept. of Physics, Durham University, South Road, Durham, DH1 3LE, UK*

<sup>3</sup>*Steward Observatory, University of Arizona, 933 N. Cherry Ave., Tucson AZ85721, USA*

<sup>4</sup>*Astronomy Center, University of Sussex, Falmer, Brighton, BN1 9QH, UK*

<sup>5</sup>*Anglo-Australian Observatory, PO Box 296, NSW 1710, Australia*

<sup>6</sup>*Institute of Computational Cosmology, Durham University, South Road, Durham, DH1 3LE, UK*

<sup>7</sup>*Department of Astronomy and Astrophysics, Pennsylvania State University, 525 Davey Laboratory, University Park, PA 16802, USA*

<sup>8</sup>*National Center for Supercomputing Applications, University of Illinois at Urbana-Champaign, 1205 W. Clark St., Urbana, IL 61801, USA*

<sup>9</sup>*School of Physics, University of New South Wales, Sydney, Australia*

<sup>10</sup>*School of Physics & Astronomy, University of St Andrews, North Haugh, St Andrews, KY16 9SS, UK*

<sup>11</sup>*Cerro Tololo Inter-American Observatory, Casilla 603, La Serena, Chile*

<sup>12</sup>*Dept. of Physics, University of Queensland, Brisbane, QLD 4072, Australia*

<sup>13</sup>*Apache Point Observatory, 2001 Apache Point Road, P.O. Box 59, Sunspot, NM 88349, USA*

<sup>14</sup>*School of Physics & Astronomy, University of Southampton Southampton, SO17 1BJ, UK*

<sup>15</sup>*Dept. of Physics and Astronomy, University of Pittsburgh, 3941 O'Hara Street, Pittsburgh, PA 15260, USA*

7 June 2018

## ABSTRACT

We present new measurements of the luminosity function (LF) of Luminous Red Galaxies (LRGs) from the Sloan Digital Sky Survey (SDSS) and the 2dF-SDSS LRG and Quasar (2SLAQ) survey. We have carefully quantified, and corrected for, uncertainties in the K and evolutionary corrections, differences in the colour selection methods, and the effects of photometric errors, thus ensuring we are studying the same galaxy population in both surveys. Using a limited subset of 6326 SDSS LRGs (with  $0.17 < z < 0.24$ ) and 1725 2SLAQ LRGs (with  $0.5 < z < 0.6$ ), for which the matching colour selection is most reliable, we find no evidence for any additional evolution in the LRG LF, over this redshift range, beyond that expected from a simple passive evolution model. This lack of additional evolution is quantified using the comoving luminosity density of SDSS and 2SLAQ LRGs, brighter than  $M_{0.2r} - 5\log h_{0.7} = -22.5$ , which are  $2.51 \pm 0.03 \times 10^{-7} \text{ L}_{\odot} \text{ Mpc}^{-3}$  and  $2.44 \pm 0.15 \times 10^{-7} \text{ L}_{\odot} \text{ Mpc}^{-3}$  respectively ( $< 10\%$  uncertainty). We compare our LFs to the COMBO-17 data and find excellent agreement over the same redshift range. Together, these surveys show no evidence for additional evolution (beyond passive) in the LF of LRGs brighter than  $M_{0.2r} - 5\log h_{0.7} = -21$  (or brighter than  $\sim L^*$ ). We test our SDSS and 2SLAQ LFs against a simple “dry merger” model for the evolution of massive red galaxies and find that at least half of the LRGs at  $z \simeq 0.2$  must already have been well-assembled (with more than half their stellar mass) by  $z \simeq 0.6$ . This limit is barely consistent with recent results from semi-analytical models of galaxy evolution.

**Key words:** cosmology: observations – galaxies: abundances – galaxies: ellipticals and lenticular, cD – galaxies: evolution – galaxies: fundamental parameters

## 1 INTRODUCTION

The formation of massive elliptical galaxies is a major conundrum in modern cosmology. Observationally, it is clear that such galaxies formed the bulk of their stars at redshifts greater than two, with evidence coming from a variety of studies, including observations of clusters and groups of galaxies (Bower et al. 1992; Ellis et al. 1997; Kodama et al. 1998; de Propris et al. 1999; Brough et al. 2002; Wake et al. 2005; Holden et al. 2005; Pimbblet et al. 2006), optical/NIR galaxy count and colour studies (Metcalf et al. 1996, 2001, 2005) and spectroscopic surveys of field galaxies over a range of redshifts (Bernardi et al. 1998; Trager et al. 2000; Bernardi et al. 2003a,b,c,d; Hogg et al. 2002; Kuntschner & Davies 1998; Baldry et al. 2004; Glazebrook et al. 2004; McCarthy et al. 2004; Cimatti et al. 2004; Thomas et al. 2005; Papovich et al. 2005; Bernardi et al. 2006).

These studies also suggest that the evolution of a majority of these massive ellipticals is consistent with a simple passive model of stellar evolution. For example, Bernardi et al. (2003c,d) have used the Sloan Digital Sky Survey (SDSS; York et al. 2000) to study the evolution of luminous early-type galaxies (out to  $z \simeq 0.3$ ) and find that, for a fixed velocity dispersion, older ellipticals are redder and fainter in luminosity, fully consistent with the expected fading of their stellar populations with time. They also find that the environment (as measured by local density) of luminous ellipticals has only a weak effect upon their properties, e.g., the Fundamental Plane fades by only 0.075 mags/arcsec<sup>2</sup> from the field to the cores of clusters (consistent with cluster galaxies forming at a slightly earlier epoch than field ellipticals). Several other studies have also found very similar results (Kuntschner et al. 2002; Clemens et al. 2006; Bernardi et al. 2006). However, several authors have found evidence for recent and/or ongoing star-formation in a fraction of local massive ellipticals (Trager et al. 2000; Goto et al. 2003; Fukugita et al. 2004; Balogh et al. 2005). This fraction appears to increase with redshift (Le Borgne et al. 2005; Roseboom et al. 2006) and decrease with mass (Caldwell et al. 2003; Nelan et al. 2005; Clemens et al. 2006).

One potential problem for studies of massive elliptical/early-type galaxies, particularly those tracking the evolution with redshift, is that of *progenitor bias* (van Dokkum & Franx 1996; van Dokkum et al. 2000). By studying only galaxies that look like massive early-type systems at high redshift, some of the progenitors of the low redshift massive early-type galaxies may be missed. An effective way to counter this problem is to study the evolution in the number density, or luminosity function (LF), of massive early-type galaxies with redshift. If these galaxies did indeed form at high redshift, then there will be little evidence for the evolution of their LF with redshift. Such studies have only just begun, e.g., the COMBO-17 (C17) survey, which reported on the evolution of  $\simeq 5000$  red (and thus implied early-type) galaxies and found at most a factor of two evolution out to  $z \simeq 1$  (corresponding to 9 Gyrs in look-back time; Bell et al. 2004). This is consistent with earlier (but smaller in number) studies of high redshift red (early-type) galaxies from the CFRS (Lilly et al. 1995; Schade et al. 1999), CNOC2 (Lin et al. 1999) and K20

(Pozzetti et al. 2003) surveys. At higher redshifts ( $z > 1$ ), recent spectroscopic surveys suggest that a significant fraction of massive galaxies are already in place at these early epochs (Glazebrook et al. 2004; Cimatti et al. 2004).

Theoretically, the existence of massive, passively-evolved ellipticals has been a major challenge for some models of galaxy evolution. For example, in the favoured hierarchical Cold Dark Matter (CDM) model of structure formation, such massive galaxies are expected to reside in the largest dark matter haloes, that form at late times through the merger of smaller mass haloes (see Kauffmann (1996) for early predictions). In recent years, there have been a number of prescriptions proposed to solve the “anti-hierarchical” nature of the formation and evolution of massive ellipticals and thus better match the observations discussed above, including: *i*) The reduction of the gas cooling rate (Benson et al. 2003); *ii*) Super-winds that eject the gas once it has cooled, but before it can form stars (Benson et al. 2003; Baugh et al. 2005); *iii*) Shock heating of infalling gas and -PdV work of the gas (Naab et al. 2005); *iv*) Feedback from Active Galactic Nuclei (AGN; Kawata & Gibson 2005; Scannapieco et al. 2005).

The latter of these proposed effects (AGN feedback) is appealing because of the observed empirical relationship between the luminosity, central concentration and mass of galactic bulges and the mass of their central super-massive black holes (Ferrarese & Merritt 2000; Tremaine et al. 2002; Novak et al. 2006). AGN feedback comes in two flavors: *i*) The merger of gas-rich galaxies causing an initial starburst, followed by the growth of the central black hole and a “quasar wind” which quenches further star-formation (Hopkins et al. 2005); *ii*) Radio feedback from low luminosity AGN that suppresses the cooling of gas in massive halos resulting in the termination of late-time star-formation (Bower et al. 2005; Croton et al. 2006). Detailed simulations of these AGN feedback models on the evolution of ellipticals has helped resolve the discrepancy between present observations and the naive hierarchical expectations of the CDM model (Springel et al. 2005; De Lucia et al. 2005; Bower et al. 2005; Hopkins et al. 2005; Croton et al. 2006). For example, De Lucia et al. (2005) predict that for galaxies more massive than  $10^{11} M_{\odot}$ , over 50% of their stars have formed by a median redshift of  $z = 2.6$ , while the typical assembly redshift of these galaxies (when these stars reside in a single object) is only  $z \simeq 0.8$ . This requires “dry mergers” of the smaller galaxies (i.e. without gas) to avoid causing bursts of new star-formation. Several authors have found evidence for such dry mergers (see van Dokkum 2005; Bell et al. 2005).

In this paper, we present an accurate measurement of the evolution of the luminosity function (LF) of Luminous Red Galaxies (LRGs; Eisenstein et al. 2001), that are predominantly massive elliptical galaxies and thus provide strong constraints on the physical mechanisms that have been suggested to produce anti-hierarchical galaxy formation in a CDM universe. We utilise two samples of LRGs, one from the SDSS ( $0.15 < z < 0.37$ ), and a new survey of higher redshift LRGs ( $0.45 < z < 0.8$ ) selected from the multi-colour SDSS photometry, but spectroscopically observed using the 2dF spectrograph on the Anglo-Australian Telescope (AAT). This new survey is known as the 2dF-SDSS LRG and QSO (2SLAQ) survey.

The LRG component of the 2SLAQ survey is a significant advance over previous surveys of massive early-type galaxies due to an increase in both the volume surveyed ( $\sim 10^7 h^{-3} \text{ Mpc}^3$ ), thus reducing the problem of cosmic variance, and the number of galaxy redshifts obtained, thus greatly increasing the statistical accuracy of the LF at bright magnitudes. In Section 2, we describe the 2SLAQ survey, while in Section 3 we present a detailed discussion of the K and evolutionary corrections, photometric errors and consistent colour selections for the SDSS and 2SLAQ samples. In Section 4.2 we present the luminosity functions of the SDSS and 2SLAQ surveys. In Section 5, we discuss our results in terms of models of galaxy evolution and conclude. Throughout, we adopt a cosmology of  $\Omega_M = 0.3$ ,  $\Omega_\Lambda = 0.7$  and  $H_0 = 70 \text{ km s}^{-1} \text{ Mpc}^{-1}$ .

## 2 LRGS IN THE SDSS AND 2SLAQ SURVEYS

We present in this paper an analysis of LRGs taken from both the SDSS survey and the 2dF-SDSS LRG and QSO (2SLAQ) survey. For the SDSS data, we only use the LRG Cut I photometric selection (using the  $g - r$  and  $r - i$  colours of galaxies) as defined and discussed in Eisenstein et al. (2001; E01). This provides us with a pseudo volume-limited sample of LRGs, with  $M_r \leq -21.8$  and  $0.15 < z < 0.35$ , selected from the SDSS Data Release (DR3, Adelman-McCarthy et al. 2005) dataset. Below  $z = 0.15$ , the space density of SDSS LRGs increases by nearly 50% because of contamination by low redshift star-forming galaxies in the colour selection, while above  $z > 0.35$ , the space density of SDSS LRGs begins to decrease because of the flux limit and the degeneracy between the colours and redshift of LRGs close to  $z \simeq 0.37$  where the  $4000\text{\AA}$  break feature passes out of the SDSS  $g$ -band into the  $r$ -band (Fukugita et al. 1996). Within the range  $0.15 < z < 0.35$ , the space density of SDSS Cut I LRGs is approximately constant with redshift (see E01).

In 2003, the 2SLAQ survey began with the goal of producing a pseudo volume-limited sample of 10,000 LRGs, with a median redshift of  $z = 0.55$ , and 10,000 faint  $z < 3$  quasars, both selected from the SDSS multi-colour imaging data. In this paper, we focus on the 2SLAQ LRGs which are selected using similar criteria as the Cut II SDSS LRGs in E01. The key differences are: (i) The apparent magnitude limit has been lowered to  $m_i(\text{model}) < 19.8$ , thus extending the volume-limited LRG samples to  $z \simeq 0.6$ ; (ii) The effective rest-frame colour cut ( $c_\perp$  in E01) has been shifted slightly bluer than in the SDSS LRG selection to accommodate the density of 2dF fibres available. This provides a less conservative colour cut, at these higher redshifts, which is essential for studying potentially small changes in their colour.

The details of the 2SLAQ LRG selection and observations are presented elsewhere (Cannon et al. 2006). However, we have measured over 11000 LRG redshifts, covering  $180\text{deg}^2$  of SDSS imaging data, from 87 allocated nights of AAT time. Over 90% of these galaxies are within the range  $0.45 < z < 0.7$ . The targeted LRGs were split into three subsamples as detailed in Cannon et al. (2006), with the primary sample (Sample 8) accounting for two thirds of these. We only focus on Sample 8 in this paper due to its high com-

pleteness and uniform selection. The overall success rate of obtaining redshifts from the 2dF spectra for Sample 8 LRGs is 95%, while the centers of the 2dF fields were spaced by  $1.2^\circ$ , resulting in an overall redshift completeness of sample 8 LRG targets of  $\sim 75\%$  across the whole survey area (see section 4.1). These data have recently been used to calibrate LRG photometric redshifts (Padmanabhan et al. 2005; Collister et al. 2006).

Although the SDSS magnitude system was designed to be on the AB scale (Fukugita et al. 1996), the final calibration has differences from the proposed values by a few percent. We have applied the corrections  $m_{AB} = m_{SDSS} + [-0.036, 0.012, 0.010, 0.028, 0.040]$  for  $u, g, r, i, z$  respectively (Eisenstein, priv. comm.). All magnitudes and colours presented throughout this paper are corrected for Galactic extinction (Schlegel et al. 1998).

## 3 SAMPLE SELECTION

The galaxy samples discussed in this paper were originally selected under the assumption that LRGs are old, passively-evolving galaxies. Here, we continue this fundamental assumption when investigating the evolution of the LRG luminosity function by applying the same passively-evolving models to our data when computing K and evolutionary (e) corrections, luminosity functions and colour selection boundaries. If this assumption is correct, then our K+e corrected luminosity functions will be identical over the whole redshift range studied here, with any additional evolution in the LRG population (beyond the simple passive model) being displayed as a change in the LF with redshift. However, as we are using two slightly different selections of LRGs to generate our total LRG sample, it is vital that we select the same galaxy population at all redshifts.

### 3.1 K+e corrections

In order to make a fair comparison between the SDSS and 2SLAQ LRG samples (at different redshifts), we must correct the properties of our observed galaxies (magnitude, colours *etc.*) into rest-frame quantities by applying K-corrections. In addition, we can also correct these rest-frame quantities for the expected evolutionary changes over the redshift range studied. These e-corrections are usually performed assuming a model for the galaxy spectral energy distribution (SED) and its evolution with redshift. In this paper, we therefore generate our K+e corrections using the Bruzual & Charlot (2003) stellar population synthesis code. In detail, we generate two stellar population models the first of which forms all its stars in a single instantaneous burst at  $z = 9.84$  (solar metallicity) and then evolves passively with no further star formation. The second model forms the bulk of its stars in a similar burst, but includes a small amount of continuous star formation throughout the rest of its evolution, accounting for 5% of its final mass. These two models are shown in Figure 1 and are labelled “Passive” and “Passive+SF” respectively.

Figure 1 shows the colour evolution as a function of redshift for these two models along with the actual measured colours of the SDSS and 2SLAQ LRGs. Some differences between the models and data are evident, e.g., the models are

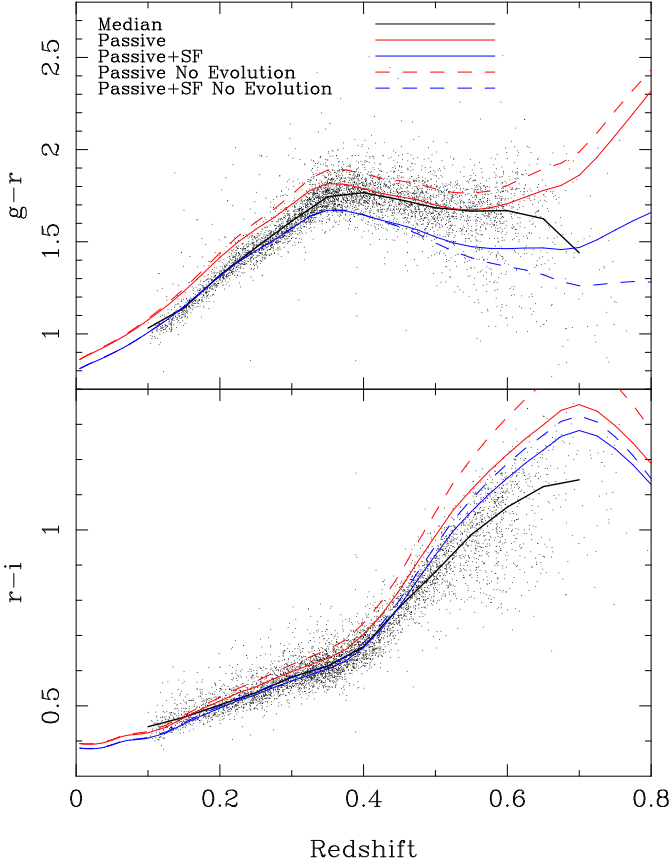


**Figure 1.** The  $g-r$  and  $r-i$  colours of the SDSS and 2SLAQ LRGs as a function of redshift (points). The solid black line shows the median of the fits with the coloured lines showing the model tracks described in the text with (solid) and without (dashed) evolution applied.

too red in  $g-r$  and too blue in  $r-i$  for the lowest redshift LRGs, with the opposite effect for the highest redshift LRGs. This offset between models and data in the lower redshift LRGs was noted in E01 and a correction to the  $g-r$  colours of 0.08 magnitudes was applied. However, with the addition of the higher redshift sample, it is clear that a simple offset is an inadequate correction over our entire redshift range. Such differences between the models and observed colours of early-type galaxies has been seen before, e.g., Wake et al. (2005) were unable to match the red sequence colours in galaxy clusters at similar redshifts, while a similar offset is seen in the colour-redshift plots of Ferreras et al. (2005) from the GOODS/CDFS fields. Simple changes to the models, such as the formation redshift, metallicity and IMF of the models, are unable to improve the model fits to the data. We also note that using the PEGASE stellar population synthesis model (Fioc & Rocca-Volmerange 1997) produced very similar results. It appears that the models are not accurately reproducing the shape of the spectrum between 4000Å and 5000Å causing an offset in  $g-r$  and  $r-i$  as the  $r$  filter passes through this (rest-frame) wavelength region. The  $g-i$  colours of LRGs are well reproduced by the models.

In order to minimise the systematic uncertainties in the models, and thus uncertainties in our K+e corrections, we

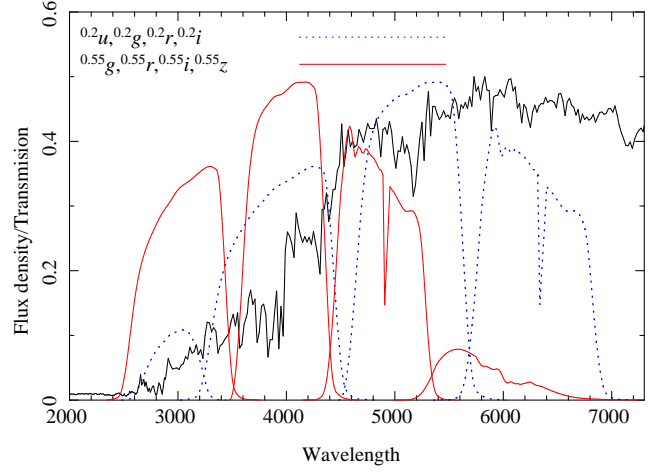


**Figure 2.** The spectral energy distribution of the passive LRG model described in the text, along with the filter transmission curves blueshifted to  $z = 0.2$  and  $z = 0.55$ .

will exploit the fact that the redshifted SDSS  $g$ ,  $r$ ,  $i$  and  $z$  passbands at  $z = 0.55$  (i.e., the median redshift of the 2SLAQ LRGs) approximately overlap the  $u$ ,  $g$ ,  $r$  and  $i$  passbands at  $z = 0.2$  (the typical redshift of a SDSS LRG). This effect is illustrated in Figure 2 where the transmission curves of the SDSS filters are plotted at  $z = 0.2$  and  $z = 0.55$  and compared to the rest-frame spectral energy distribution of our passively evolved stellar population model as discussed above.

Therefore, for each LRG, we estimate its K+e correction by interpolating between the two SED models using the observed  $g-i$  colour of the galaxy. For the SDSS LRG sample, we simply correct the observed  $g$ ,  $r$  and  $i$  magnitudes to  $g$ ,  $r$  and  $i$  at  $z = 0.2$ . The median size of these K+e corrections ranges from 0.01 in  $i$  passband to 0.43 in  $g$ -band. For the 2SLAQ LRG sample, we again use the observed  $g-i$  colour to interpolate between the two SED models, but this time correct from observed  $r$ ,  $i$  and  $z$  passbands to  $g$ ,  $r$  and  $i$  at  $z = 0.2$ . The median size of these K and K+e corrections are 0.32 and 0.7 respectively when going from the  $r$ -band to the  $g$ -band, 0.1 and 0.4 going  $i$ -band to  $r$ -band, and 0.1 and 0.4 when correcting from  $z$ -band to  $i$ -band. Tables of these corrections for the two different SED models are given in Appendix A.

Throughout the rest of this paper, we use the notation  $M_{0.2r}$  to represent the absolute magnitude of an LRG observed through a SDSS  $r$ -band filter redshifted to 0.2. This notation is similar to that used in Blanton et al. (2003), except here we include an evolutionary correction in addition to the K-correction. We note that  $M_{0.2r} \simeq M_r(z=0) + 0.11$  for the colour of a typical LRG.

### 3.2 Consistent Colour Selection

The differences in the SDSS and 2SLAQ selection criteria discussed above are explicitly illustrated in Figure 3. Here, we have taken a sample of SDSS main galaxies (Strauss et al. 2002) with  $0.1 < z < 0.2$  and K+e corrected all of them to  $z = 0.2$ . The SDSS main sample consists of all galaxies with  $r < 17.77$  and provides a representative sample

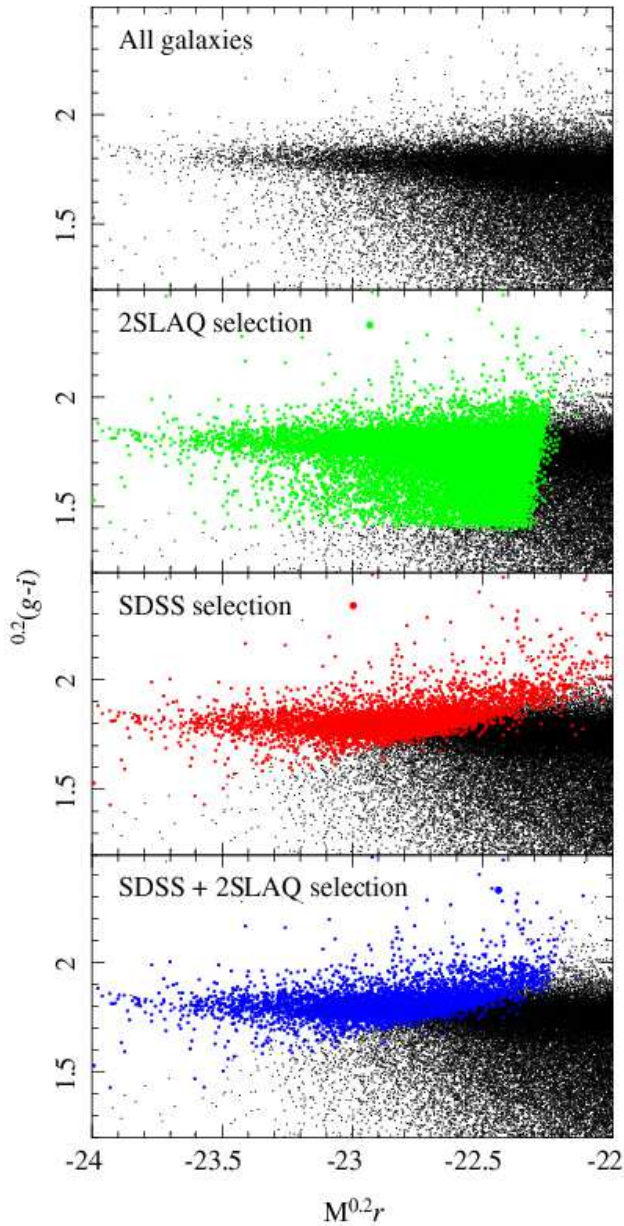


**Figure 3.** The  $^{0.2}(g-i)$  versus  $M_{0.2r}$  colour magnitude relation for SDSS main galaxies with  $0.1 < z < 0.2$  all K+e corrected to  $z = 0.2$ . The small black points in each panel show the whole sample. The second panel shows those galaxies that would have been selected by the 2SLAQ selection criteria when K+e corrected to  $z = 0.55$  (large points). The third panel shows those galaxies that would be selected by the SDSS LRG Cut I selection criteria when K+e corrected to  $z = 0.2$  (large points). The final panel shows the galaxies that satisfy both the SDSS and 2SLAQ LRG selection criteria at both  $z = 0.2$  and  $0.55$  respectively (large points).

of the whole galaxy population. For this sample, we generate the K+e corrections by interpolating between a passive model and one with continuous star formation based on the observed  $g-i$  colour of the galaxy. We then applied the SDSS and 2SLAQ LRG selection criteria at the two redshifts respectively. We plot in Figure 3 the colour-magnitude relation ( $^{0.2}(g-i)$  versus  $M_{0.2r}$ ) for these galaxies, where  $^{0.2}g$

is the  $g$  filter at  $z = 0.2$ , illustrating which galaxies would be selected by each criteria and their combination. This figure clearly illustrates the bluer 2SLAQ selection as well as the magnitude dependence of the SDSS LRG colour selection (E01) as the selection cuts through the red sequence starting at  $M_{0.2r} > -22.8$ .

Although the detailed colour evolution of LRGs remains unknown, we will proceed by assuming a simple passive model for LRGs evolution and thus make a self-consistent colour selection at both  $z = 0.2$  and  $z = 0.55$ . We can then check whether the observed LF evolution is consistent with this simple hypothesis and whether any further evolution (beyond passive) is required to explain our observations. To do this, we first use the K+e corrections described above to correct all the LRGs in both samples to the redshift of the other sample *i.e.* we correct the 2SLAQ LRGs to  $z = 0.2$  and the SDSS LRGs to  $z = 0.55$ . We then require that for any individual LRG to be included in our analysis of the LRG LF it must satisfy both the SDSS criteria (at  $z = 0.2$ ) and the 2SLAQ criteria (at  $z = 0.55$ ). As might be expected, considering the broader colour and magnitude ranges of the 2SLAQ selection criteria, most of the SDSS LRGs ( $\approx 90\%$ ) would still be selected as LRGs at  $z = 0.55$ . The opposite is not true with only  $\approx 30\%$  of the 2SLAQ LRGs satisfying the stricter SDSS Cut I LRG criteria.

Figure 4 shows the colour distributions of all the 2SLAQ LRGs (red) and all the SDSS LRGs (blue) convolved with the typical photometric errors of the 2SLAQ LRGs, K+e corrected to  $z = 0.2$ . The left-hand panel shows the colour distributions of the full sample of SDSS and 2SLAQ LRGs considered in this paper (*i.e.*, the raw data), while the middle panel shows only those galaxies which satisfy both the SDSS and 2SLAQ LRG selection criteria at  $z = 0.2$  and  $z = 0.55$  respectively. As mentioned previously, the 2SLAQ LRGs in the left-hand panel have bluer colour distributions compared to the SDSS LRGs, reflecting their bluer and fainter selection criteria. When the joint SDSS and 2SLAQ selection criteria are applied, the colour distributions of this restricted set of 2SLAQ LRGs now become redder and much closer to the SDSS LRG colour distributions. However, an offset between the 2SLAQ and SDSS LRG colour distributions is still evident (in the middle panel), *i.e.*,  $0.05$  magnitudes in the mean  $g-r$  colour of LRGs. We believe this offset is due to residual inaccuracies in the models used for our K-corrections, although we have tried to reduce this problem by correcting between overlapping filters. The wide redshift range of our samples (particularly in the SDSS) results in the errors in our K-corrections still being significant and detectable.

To improve the agreement between the 2SLAQ and SDSS LRG samples, we restrict the redshift ranges of these two samples to be closer to the redshifts where the SDSS filters have their greatest overlap (Figure 2). We restrict the SDSS LRG sample to  $0.17 < z < 0.24$  and 2SLAQ LRG sample to  $0.5 < z < 0.6$ , which reduces the amplitude of the K-corrections at  $z = 0.2$  for the SDSS LRGs to a range of  $0.005$  to  $0.06$ , compared to  $0.01$  to  $0.11$  without this restricted redshift range. Likewise, the amplitude of the 2SLAQ LRG K-corrections reduce to a range of  $0.08$  to  $0.30$ , compared to  $0.11$  to  $0.36$  without the restricted redshift range. The right-hand panel of Figure 4 shows the colour distributions of LRGs that satisfy both the SDSS and 2SLAQ selection criteria within the restricted redshift



**Table 1.** The median photometric errors for the SDSS and 2SLAQ LRGs from the single-epoch SDSS photometry and the multi-epoch SDSS photometry described in the text.

	<i>u</i>	<i>g</i>	<i>r</i>	<i>i</i>	<i>z</i>
SDSS single-epoch	0.56	0.04	0.01	0.01	
2SLAQ single-epoch		0.15	0.05	0.03	0.09
2SLAQ multi-epoch		0.05	0.02	0.01	0.03

ranges discussed above. This results in the colour distributions of the two LRG samples being almost identical; the median colour difference is now less than 0.01 magnitudes. These restricted redshift LRG samples give us greater confidence that, under the assumption of passive evolution, we are now selecting the same type of galaxy in both the SDSS and 2SLAQ surveys. It also suggests that the discrepancy between the observed and model colours is only affecting the K-corrections and not the evolution corrections. The final redshift-restricted samples contain 6326 SDSS LRGs, with  $0.17 < z < 0.24$ , and 1725 2SLAQ LRGs, with  $0.5 < z < 0.6$ . Clearly making such tight redshift cuts has resulted in a significant reduction in the size of our samples. However, we believe that minimising the errors in the K+e corrections is vital to ensure that the LRG samples from the SDSS and 2SLAQ are as close as possible.

### 3.3 Photometric errors

Another potential bias that could affect the sample selection is the larger photometric errors on the 2SLAQ LRGs compared to the SDSS LRGs (because they are intrinsically fainter and from the same imaging dataset). This could systematically change the selection, as a function of redshift, as more 2SLAQ LRGs could be scattered both in and out of the sample as the photometric error increases.

We attempt to measure this effect by utilising the multi-epoch SDSS imaging data available over a subsample of the 2SLAQ survey area (see Baldry et al. 2005; Scranton et al. 2005). This multi-epoch data covers a total of  $\simeq 190$  deg<sup>2</sup> of the southern part of the 2SLAQ survey, and provides better signal-to-noise photometry for LRGs in this area as demonstrated by Table 1. We begin by comparing the number of LRGs that satisfy the 2SLAQ selection criteria using both the single and multi-epoch photometry. We find that 10059 2SLAQ LRG targets were selected from the single-epoch photometry compared to 10265 2SLAQ LRG targets selected using the multi-epoch data. However, 25% of these targets are different between the two samples and have been scattered across the selection boundaries in almost equal numbers. In Figure 5, we show the colour-magnitude relationship for LRGs both in common between the multi and single-epoch photometry as well as the LRGs only selected in one of the two data sets. As expected, LRGs selected only in the single-epoch data (i.e., missed by the 2SLAQ selection using the multi-epoch photometry) are fainter and bluer than 2SLAQ LRGs scattered out of the single-epoch selection but selected using the multi-epoch photometry (the right-hand panel of Figure 5). We note however that the colour-magnitude relationship of LRGs for both the multi and single-epoch photometry is nearly identical for  $i < 19.3$ .

This magnitude corresponds to  $M_{0.2,r} = -23.0$  at  $z = 0.6$ , the upper redshift limit used herein to calculate the luminosity function.

As a further test, we can limit this comparison, to only LRGs with measured redshifts. This is possible because a subset of the 2dF fibres ( $\sim 30\%$ ) were allocated to galaxy targets that lie slightly beyond the original 2SLAQ colour selection boundaries for the highest priority “Sample 8” selection (for details see Cannon et al. 2006). These extra LRG redshifts allow us to investigate the effect of photometric errors on the completeness of “Sample 8”, although we are limited by the small size of the colour region beyond sample 8 when considering those galaxies that weren’t selected but should have been. In Figure 6 (top), we show the multi-epoch colour and magnitude distributions for 2SLAQ LRGs, in the redshift range  $0.5 < z < 0.6$ , all K+e corrected to  $z = 0.2$  as before. As above, 22% of the 2SLAQ LRGs are scattered into the sample because of photometric errors, i.e., they satisfy the selection criteria in the single-epoch photometry, but fail the criteria for the multi-epoch photometry. Again, these LRGs are bluer and fainter (in absolute magnitude) as shown by the dotted blue line in Figure 6 (top). However, brighter than  $M_{0.2,r} < -22.65$  the magnitude distributions of those selected by the single and multi-epoch data are almost identical. We are therefore confident that the photometric errors have minimal effect on the 2SLAQ sample function brighter than this limit.

A more significant effect of the photometric errors occurs when we apply the additional selection criteria we use to match the samples as discussed in Section 3.2. We can again try to quantify this effect using the multi-epoch data and again show in Figure 6 (centre) the magnitude distributions of the single and multi-epoch selected 2SLAQ LRGs. However, here we only show those LRGs in the redshift range  $0.5 < z < 0.6$  that pass both both the SDSS and 2SLAQ selection criteria. Unlike previously, where we had a limited set of spectra for galaxies beyond the selection boundaries, in this instance we have many galaxies far beyond the selection boundaries due to the much bluer and fainter 2SLAQ selection. This is clearly visible when comparing the second and fourth panels of Figure 3. On inspection of the magnitude distributions in Figure 6 it is clear that a significant fraction of galaxies are being scattered across the selection boundaries even for LRGs as bright as  $M_{0.2,r} = -23.3$ . This is more clearly illustrated by the bottom panel of Figure 6 where we plot the ratio of the number of LRGs selected using the multi-epoch data to the number selected using the single-epoch data as a function of absolute magnitude. Since we are confident that we have fully sampled the colour-magnitude space beyond the selection boundaries we can use this ratio to correct the luminosity function and integrated number and luminosity densities presented in the Section 4.2. We note that the only place that we are not sampling beyond the boundary is for the faintest and reddest objects and we are thus not confident of the correction and any resulting quantities for  $M_{0.2,r} > -22.4$ . In order to generate accurate errors on this correction, we take the multi-epoch selected sample and add random Gaussian errors typical of the 2SLAQ photometric errors to each magnitude. We then calculate how many LRGs would be selected in our final sample. We repeat this procedure 10000 times and measure

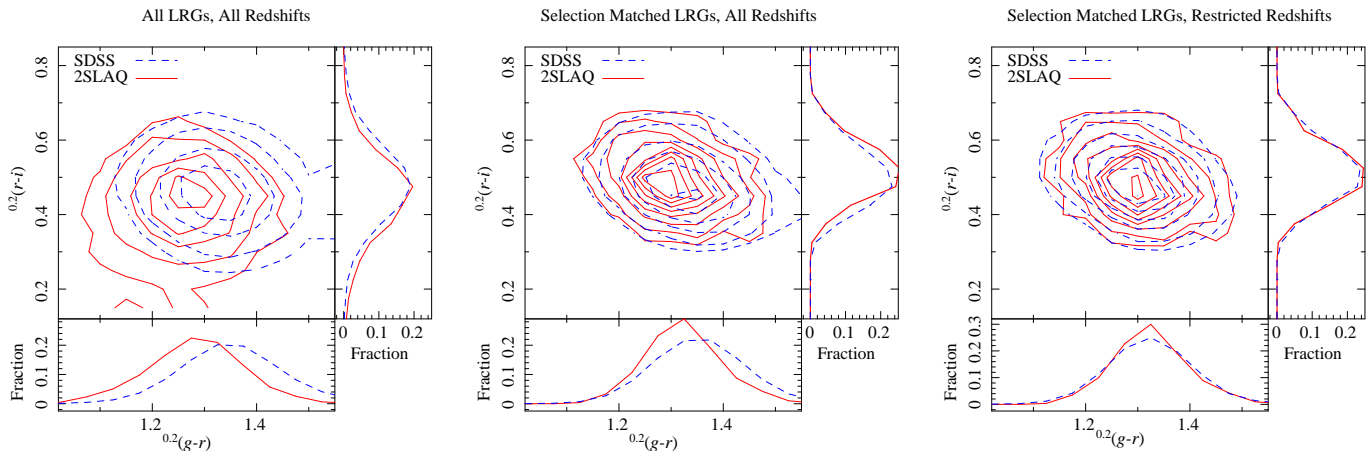


**Figure 4.** The  $g-r$  and  $r-i$  colours of all the SDSS and 2SLAQ LRGs K+e corrected to  $z = 0.2$ . The SDSS distributions have been convolved with the typical 2SLAQ photometric errors. The left-hand plot shows all the LRGs in these two samples, while the middle plot shows only those LRGs (in both samples) that match both the SDSS and 2SLAQ LRG selection criteria (described in the text). The right-hand plot shows those LRGs that match both the SDSS and 2SLAQ LRG selection criteria and have an additional redshift restriction;  $0.17 < z < 0.24$  for the SDSS LRGs and  $0.5 < z < 0.6$  for the 2SLAQ LRGs.

the standard deviations in each bin which are shown as the errors in Figure 6 (bottom).

So far we have only discussed the effect of the photometric errors on the 2SLAQ LRGs. It is also worth briefly discussing any potential effect on the SDSS LRGs. As listed in Table 1 the typical photometric errors on the SDSS LRGs are much smaller than those of 2SLAQ and comparable to the multi-epoch errors on the 2SLAQ LRGs, except in the case of the  $u$  band. However, the  $u$  band data are only used when applying the 2SLAQ selection criteria to the SDSS LRGs and since the 2SLAQ criteria are typically significantly bluer and fainter than the SDSS criteria one would expect a small effect. In fact only 5% of the SDSS LRGs are removed when the 2SLAQ criteria are applied to them and most of these (3%) are as a result of the 2SLAQ magnitude limits where the  $r$  band magnitude is used. We are therefore confident that the photometric errors on the SDSS LRGs result in an insignificant amount of scattering across the selection boundaries.

## 4 LUMINOSITY FUNCTIONS

### 4.1 Redshift Completeness

The 2SLAQ survey is not spectroscopically complete unlike the SDSS LRG sample which is  $> 99\%$  complete for input target redshifts. Therefore, we must correct the 2SLAQ survey for this redshift incompleteness, taking into account any dependence on magnitude and/or colour. The redshift completeness is defined as the ratio of the number of Sample 8 2SLAQ LRGs with a reliable redshift to the number of Sample 8 target LRGs selected from the SDSS imaging in each observed 2dF field. To calculate this, we need to define the exact survey area covered by the 2SLAQ survey in order to determine the number of possible LRG targets. To achieve this, we repeatedly ran the 2dF configuration software on random positions until we had configured over 5 million random points in a single 2dF field. This exercise provides a

detailed map of all possible positions available to the 2dF fibres within the field of view. We then built a random catalogue for the whole 2SLAQ survey area by placing this single randomised 2dF field at every observed field centre (see Cannon et al. 2006). Finally, we remove any regions not in the original target input catalogue, i.e., edges of the 2dF fields, that extended beyond the SDSS photometry, and holes in the SDSS coverage. This produced a random catalogue of approximately 400 million positions, covering every possible position a 2dF fibre could have been placed throughout the whole 2SLAQ survey. We then pixelised these random positions (into 30 by 30 arcsecond pixels) to generate a survey mask and positively flagged all pixels that contain at least one random position.

The survey mask was used in two ways. First, we calculated the area of the survey by summing all positive pixels, giving an area of  $180.03 \text{ deg}^2$ . Secondly, we used the mask to define those LRGs in the input catalogue that could have been included in the 2SLAQ survey in order to calculate the redshift completeness. We also restrict the observed LRGs in the same manner resulting in about 0.5% of the observed LRGs (with redshifts) being excluded. This is caused by slight changes made to the 2dF configuration software during the 2SLAQ survey which we are unable to account for when constructing our mask. Figure 7 shows the redshift completeness of the 2SLAQ survey as a function of magnitude and colour. There are no significant dependence of the redshift completeness on the  $r-i$  colour, and  $i$  magnitude only shows any significant dependence fainter than  $i = 19.7$ . However, we do witness a dependency on the  $g-r$  colour of the LRGs. We correct for this dependence by fitting a 3rd order polynomial to the data (as shown in Figure 7) and use this function to calculate the completeness for each LRG depending on its observed  $g-r$  colour. Including this correction changes the 2SLAQ LRG LF by  $< 1\%$  compared to assuming an overall redshift completeness of 76.5% regardless of its  $g-r$  colour.

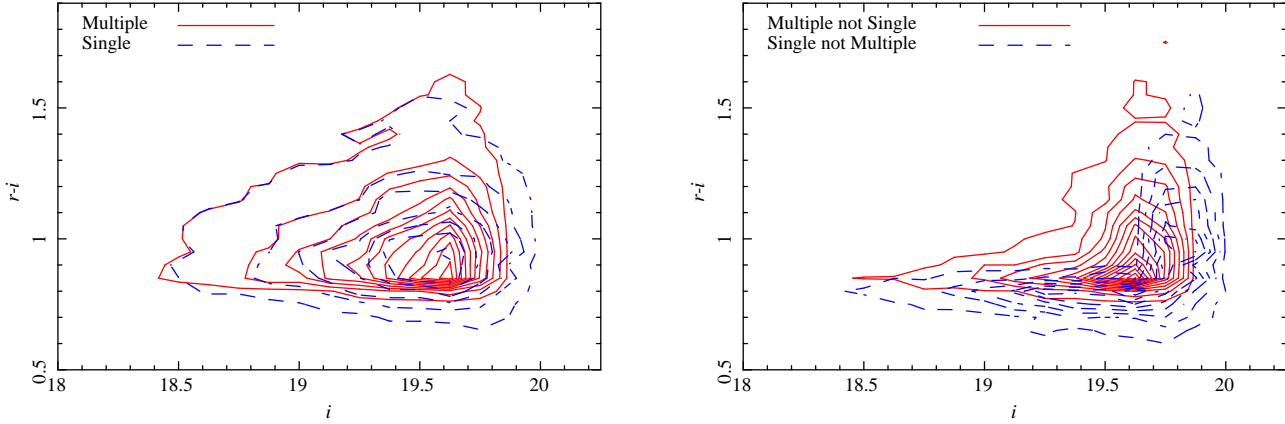


**Figure 5.** The colour–magnitude relationship for LRGs satisfying the 2SLAQ selection criteria. We only show here LRGs within the 2SLAQ survey area covered by the SDSS multi-epoch photometry. The magnitudes used here were taken from the multi-epoch photometry as they are better signal-to-noise (Table 1). The left-hand panel shows LRGs that satisfy the 2SLAQ selection criteria for the single-epoch (dashed contours) and multi-epoch photometry (solid contours). The right-hand panel shows LRGs only selected in one of the two sets of photometry; red solid contours are LRGs selected in the multi-epoch photometry but missed in the single-epoch photometry, and visa-versa for the blue dashed contours.

**Table 2.** The  $M_{0.2r}$  luminosity function with evolutionary corrections for the SDSS and 2SLAQ LRGs. The values of  $M_{0.2r}$  are the median of the bins, the density is given in units of  $10^{-6} \text{ Mpc}^{-3} \text{ mag}^{-1}$  and the errors are 1 sigma.

SDSS		2SLAQ	
$M_{0.2r}$	Density	$M_{0.2r}$	Density
-24.45	$0.03 \pm 0.03$	-24.55	$0.20 \pm 0.19$
-24.17	$0.15 \pm 0.06$	-24.20	$0.32 \pm 0.20$
-23.94	$0.62 \pm 0.11$	-23.91	$0.63 \pm 0.24$
-23.68	$1.91 \pm 0.19$	-23.68	$1.99 \pm 0.42$
-23.44	$6.51 \pm 0.34$	-23.43	$7.72 \pm 1.03$
-23.19	$17.56 \pm 0.55$	-23.21	$15.45 \pm 1.81$
-22.96	$34.47 \pm 0.76$	-22.96	$30.59 \pm 3.11$
-22.75	$32.59 \pm 0.75$	-22.73	$32.25 \pm 3.59$
-22.52	$10.47 \pm 0.44$	-22.50	$16.94 \pm 2.44$
-22.32	$0.86 \pm 0.14$	-22.33	$1.19 \pm 0.70$

**Table 3.** The  $M_{0.2r}$  luminosity function without evolutionary corrections for the SDSS and 2SLAQ LRGs. The values of  $M_{0.2r}$  are the median of the bins, the density is given in units of  $10^{-6} \text{ Mpc}^{-3} \text{ mag}^{-1}$  and the errors are 1 sigma.

SDSS		2SLAQ	
$M_{0.2r}$	Density	$M_{0.2r}$	Density
–	–	-24.86	$0.20 \pm 0.19$
–	–	-24.59	$0.14 \pm 0.13$
-24.46	$0.03 \pm 0.03$	-24.41	$0.45 \pm 0.22$
-24.14	$0.23 \pm 0.07$	-24.13	$0.78 \pm 0.27$
-23.90	$0.76 \pm 0.12$	-23.89	$4.50 \pm 0.62$
-23.63	$2.84 \pm 0.22$	-23.67	$12.18 \pm 1.30$
-23.39	$7.96 \pm 0.37$	-23.41	$22.29 \pm 1.83$
-23.15	$22.15 \pm 0.61$	-23.17	$31.95 \pm 2.05$
-22.92	$36.64 \pm 0.78$	-22.92	$26.79 \pm 2.88$
-22.71	$27.68 \pm 0.69$	-22.71	$9.54 \pm 2.34$
-22.47	$6.96 \pm 0.36$	–	–

## 4.2 The Luminosity Function

In Figure 8, we present the  $M_{0.2r}$  luminosity function (LF) of the 2SLAQ and SDSS LRG samples as described above, both without (top panel) and with (bottom panel) passive evolution corrections. We calculated these LFs using the  $1/V_{\text{max}}$  method, where for each galaxy we compute the maximum and minimum redshifts at which it would have been selected, including the K+e corrections described above. For all LRGs brighter than  $M_{0.2r} = -23$ , the maximum and minimum redshifts correspond to redshift limits described previously, namely  $0.17 < z < 0.24$  for the SDSS sample and  $0.5 < z < 0.6$  for the 2SLAQ sample. Therefore, above this absolute magnitude, both samples are essentially volume-limited. The luminosity functions were then determined by calculating the volume ( $V_{\text{max}}$ ) within which each galaxy is detectable, modified by the colour-dependent redshift completeness corrections for the 2SLAQ sample, and summed over all galaxies in the sample. We then apply the photometric error scattering corrections discussed in Section 3.3

to each bin. We provide the numerical values of the SDSS and 2SLAQ LFs in Tables 2 and 3.

We use jack-knife (JK) re-sampling to calculate the errors on our luminosity functions. This is achieved by splitting the SDSS and 2SLAQ samples into 20 subregions, of equal area, and re-calculating 20 LFs with each of these subregions removed in turn. We find that for the 2SLAQ sample the JK errors are up to 30% larger than the Poisson errors in the four faintest magnitude bins (those which contain the most galaxies), while the two error estimates are the same for the brighter bins. We therefore quote in Tables 2 and 3, and plot in Figure 8, the larger of these two errors combined with the errors introduced by the photometric error scattering correction. For the SDSS sample, we find that the JK errors are consistent with the Poisson errors for all magnitude bins; we therefore use the Poisson errors.

Table 4 lists the integrated number and luminosity densities for a series of magnitude limits for the 2SLAQ and SDSS samples and their ratio. These are again corrected for



**Table 4.** The integrated number and luminosity density of the evolution corrected SDSS and 2SLAQ samples and the ratio of these two measurements.

Sample	Density ( $\times 10^{-6}$ Mpc $^{-3}$ )			Luminosity Density ( $\times 10^6$ L $_{\odot}$ Mpc $^{-3}$ )		
	M $_{0.2r} < -22.5$	M $_{0.2r} < -23.0$	M $_{0.2r} < -23.5$	M $_{0.2r} < -22.5$	M $_{0.2r} < -23.0$	M $_{0.2r} < -23.5$
SDSS	25.09 $\pm$ 0.33	9.77 $\pm$ 0.20	1.12 $\pm$ 0.07	3.62 $\pm$ 0.05	1.79 $\pm$ 0.04	0.31 $\pm$ 0.02
2SLAQ	24.36 $\pm$ 1.47	9.33 $\pm$ 0.68	1.24 $\pm$ 0.16	3.53 $\pm$ 0.21	1.78 $\pm$ 0.12	0.36 $\pm$ 0.05
Ratio	1.03 $\pm$ 0.06	1.05 $\pm$ 0.08	0.91 $\pm$ 0.13	1.03 $\pm$ 0.06	1.01 $\pm$ 0.08	0.86 $\pm$ 0.13

the effect of the photometric errors scattering galaxies into and out of the sample. However, in this instance we use the fit to the relation shown in Figure 6 as we need to make a correction to each individual galaxy. The errors are again a combination of the JK errors and those from the photometric scattering.

## 5 DISCUSSION

As seen in Figure 8, the SDSS and 2SLAQ LFs brighter than M $_{0.2r} = -22.6$  are in excellent agreement when the passive evolution corrections are included. Fainter than this limit we are not confident of the photometric scattering correction we have made, although we note that the LFs are still in reasonable agreement. The agreement of these luminosity functions is further confirmed by calculating the integrated number and luminosity density of LRGs as given in Table 4. Brighter than M $_{0.2r} = -22.5$ , both the integrated luminosity and number density of the 2SLAQ and SDSS samples agree to within their one sigma errors, and are measured to better than 10% out to  $z = 0.6$ .

Throughout the analysis presented herein, we have consistently used the same simple passive evolution model for predicting and correcting the colours and luminosities of LRGs as a function of redshift, and this agreement demonstrates the lack of any extra evolution, beyond the passive fading of old stars, out to  $z \simeq 0.6$ . This result confirms the underlying assumptions of Eisenstein et al. (2001), and Cannon et al. (2006), that the majority of LRGs out to  $z \simeq 0.6$  can be selected via straightforward colour cuts, in multicolour data, assuming simple passive evolution of their stellar populations. The result also confirms the work of Bernardi et al. (2003c,d) for lower redshift massive ellipticals in the SDSS.

It may appear that our lack of extra evolution beyond passive (out to  $z \sim 0.6$ ) is in conflict with recent results from the C17, DEEP2, and SXDS surveys (Bell et al. 2004; Faber et al. 2005; Yamada et al. 2005). These smaller-area, but deeper (in magnitude limit and redshift), surveys find evidence for a change in the density of red galaxies out to  $z \sim 1$  beyond that expected from passive fading of the stellar populations. For example, Faber et al. (2005) report a quadrupling of  $\phi^*$  for red galaxies since  $z = 1$ , although this result is strongest in their highest redshift bin, where they admit their data are weakest. A direct comparison with these deeper surveys is difficult because of the differences in colour selections used for the surveys, as well as the relative luminosity ranges probed by the different surveys, i.e., the 2SLAQ survey is designed to probe galaxies brighter than a few  $L^*$ , while the DEEP2, SXDS and C17 surveys

effectively probe galaxies below  $L^*$  at  $z \sim 0.6$  (due to their smaller areal coverage and fainter magnitude limits).

However, to facilitate such a comparison, we show in Figure 9, the LFs from Figure 8, and the C17 red galaxy LFs (Bell et al. 2004, Figure 3) for the same redshift range and K+e corrected to M $_{0.2r}$ . We only plot our LFs to M $_{0.2r} < -22.9$  as we do not include all the red galaxies fainter than this due to the SDSS LRG selection criteria. Figure 9 demonstrates that when one restricts the data to the same redshift range, there is excellent qualitative agreement between the 2SLAQ and C17 luminosity functions. We are unable to make a quantitative comparison due to the difficulty in exactly matching the selection criteria of the two surveys. Taken together, the surveys shown in Figure 9 extend the evidence for no evolution in the LF of LRGs to M $_{0.2r} < -21$ , which is close to  $L^*$  in the LF. Figure 9 also demonstrates that these two surveys are probing different luminosity regimes at  $z < 0.6$  as there is at most only 0.5 magnitudes of overlap in their LFs in which the C17 survey is becoming seriously affected by small number statistics due to its smaller areal coverage.

The C17 data presented in Figure 9 agrees with our findings that for the brightest galaxies there appears to be no evidence for density evolution out to  $z \sim 0.6$ . This result is not necessarily in conflict with the work of Bell et al. (2004); Faber et al. (2005); Yamada et al. (2005), as we are still probing different redshift and luminosity ranges than these other studies. Taken together, these results could indicate the existence of different evolutionary scenarios above and below  $L^*$  in the luminosity function, i.e., above  $L^*$ , galaxies have only evolved passively (since  $z = 0.6$ ), while below this luminosity, the red galaxy population is experiencing significant evolution. Kodama et al. (2004) sees similar evidence for differential evolutionary trends with luminosity at  $z \sim 1$ , and claim this supports the idea of “down-sizing” i.e., the galaxy evolutionary processes (like star-formation and assembly) decrease with increased luminosity as a function of redshift. These higher redshift observations are also consistent with the observed transition, at  $M_r \sim -20.5$ , in the local colour-magnitude relationship between a dominant “red” population of galaxies (above this luminosity), compared to “blue” population below. Likewise, Kauffmann et al. (2003) find a significant change in the distribution of stellar masses of local galaxies at the same luminosity. A more detailed joint analysis of the 2SLAQ and deeper surveys will be presented in a forthcoming paper.

The luminosity functions given in Figure 8 place tight constraints on models of massive galaxy formation and evolution. Our results appear to favour little, or no, density evolution, as we only require the expected passive evolution of the luminosities of these LRGs to explain the observed

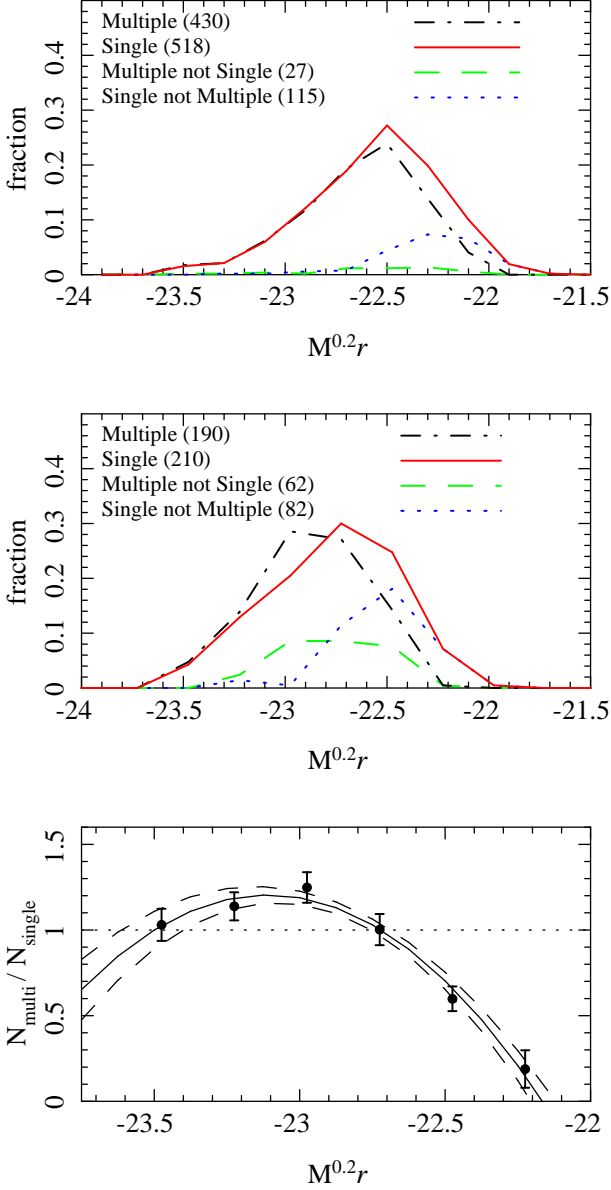


**Figure 6.** Top and Middle - The magnitude distributions for all 2SLAQ LRGs in the redshift range  $0.5 < z < 0.6$  with multi-epoch photometry. This subsample is further split into LRGs selected from the multi-epoch data (dot-dashed line), from the single-epoch data (solid line), and those LRGs selected only from multi-epoch data but not the single epoch data (dashed line) and visa-versa (dotted line). The distributions are normalised to the number in the single-epoch subsample. The number of LRGs in each of these subsamples is given in parentheses in the top panel. The top panel shows those passing the original 2SLAQ selection criteria, the middle those passing the additional selection criteria discussed in Section 3.2. Bottom - The ratio of number selected using the multi-epoch data to the number selected using the single epoch data using the additional selection criteria discussed in Section 3.2. The solid line shows a polynomial fit and the dashed lines the 1 sigma errors on the fit.

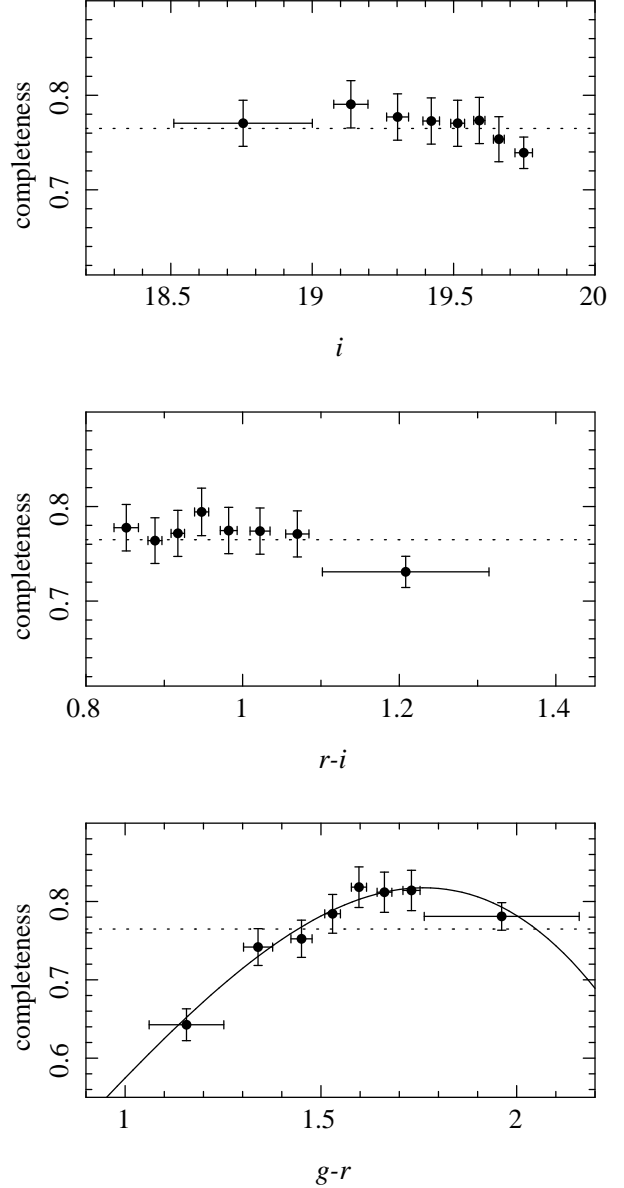


**Figure 7.** The redshift completeness of 2SLAQ LRGs as a function of apparent  $i$  magnitude (top panel),  $r - i$  colour (middle panel) and  $g - r$  colour (bottom panel). The solid line in the bottom panel shows the 3rd order polynomial fit to the data and used to correct the sample for this incompleteness as a function of  $g - r$  colour. The bins, chosen to contain 800 LRGs each, are plotted at the mean magnitude of the bin with the one sigma error bars.

differences in their LFs as a function of redshift. In other words, there are already enough LRGs per unit volume at  $z \simeq 0.6$  to account for the density of LRGs measured at  $z \simeq 0.2$ . To study this further, we must compare our results with the latest predictions for massive galaxy evolution. For example, De Lucia et al. (2005) have used the effects of AGN feedback to regulate new star-formation in massive ellipticals within their semi-analytical Cold Dark Matter (CDM) model of galaxy formation. As shown in Figures 4 & 5 of De Lucia et al. (2005), they find that 50% of stars in  $z = 0$  massive ellipticals are already formed by a

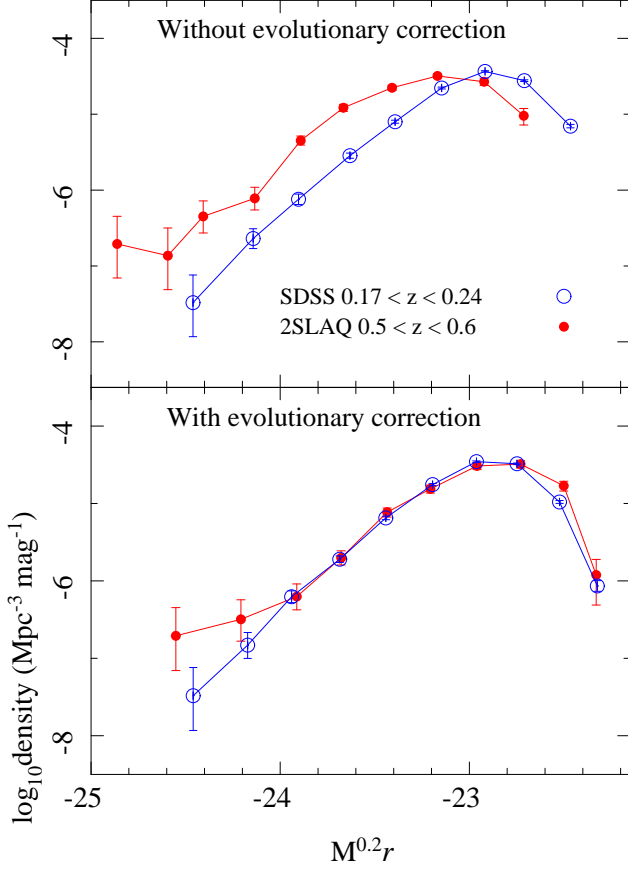


**Figure 8.** The  $M_{0.2r}$  luminosity function without (top panel) and with (bottom panel) passive evolution corrections for both the SDSS (open data points) and 2SLAQ (solid data points) LRG samples. The points are plotted with their one sigma error bars as described in the text.

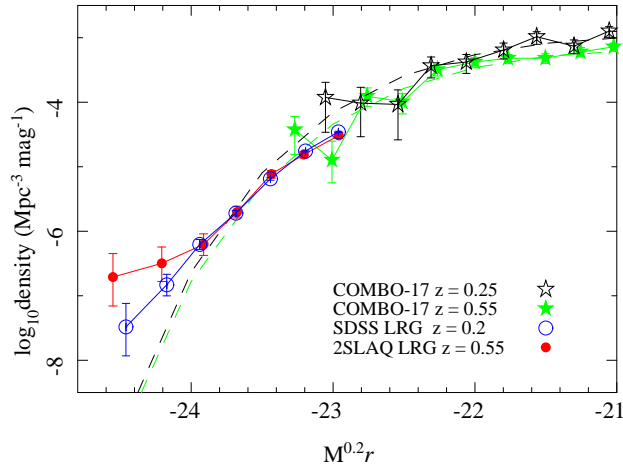


**Figure 9.** The  $M_{0.2r}$  luminosity function with passive evolution corrections for the SDSS (blue open data points), 2SLAQ (red solid data points) LRG samples, and the COMBO-17 red galaxies at  $z = 0.25$  (black open stars) and  $z = 0.55$  (green solid stars) (Bell et al. 2004). The dashed lines show the Schechter function fit to the COMBO-17 points. The points are plotted with their one sigma errors.

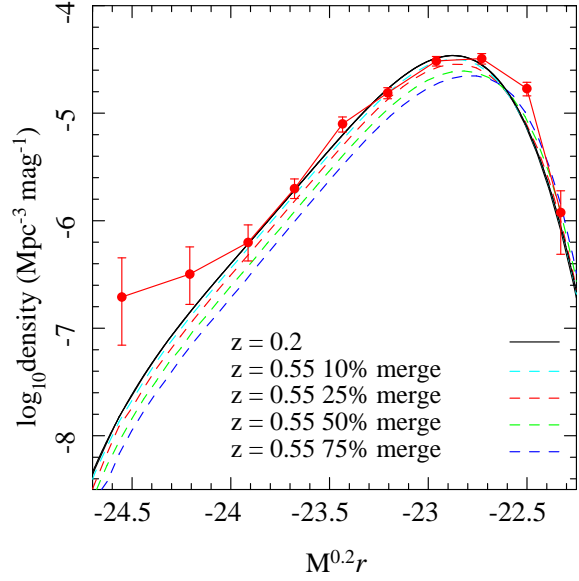


**Figure 10.** The  $M_{0.2r}$  luminosity function with passive evolution corrections for the 2SLAQ LRGs (solid data points) and fit to the SDSS LRGs black line. The lines show the effect of splitting varying fractions of the 2SLAQ LRGs in two, simulating major mergers between  $z = 0.6$  and  $z = 0.2$ .

**Table 5.** The chi-squared values for fitting difference merger fractions

Fraction Merging	$M_{0.2r} < -22.75$		$M_{0.2r} < -23.25$	
	Reduced $\chi^2$	Prob	Reduced $\chi^2$	Prob
0	0.68	0.70	0.53	0.76
0.10	0.64	0.74	0.90	0.47
0.25	1.66	0.10	2.00	0.07
0.50	4.54	< 0.0001	3.52	0.003
0.75	6.07	< 0.0001	6.08	< 0.0001

median redshift of  $z = 2.6$ , yet 50% of the stellar mass of  $z = 0$  massive ellipticals is not in place until a median redshift of  $z = 0.8$ . In Figure 9 of their paper, they show that galaxies more massive than  $\simeq 10^{11} M_{\odot}$  are built up through  $\sim 5$  major mergers, that must be “dry” (without gas) to prevent new star-formation (van Dokkum 2005). Using the Bruzual & Charlot (2003) models described earlier, we estimate that our LRGs have stellar masses  $> 5 \times 10^{11} M_{\odot}$ , consistent with the massive galaxy sample discussed by De Lucia et al. (2005).

We investigate a simple model, motivated by the idea of “dry mergers” and the results of De Lucia et al. (2005), to simulate the effect on the luminosity function of the hierarchical build-up of these LRGs through major merger events. To achieve this, we fit the SDSS LRG LF predict the higher redshift (at  $z = 0.55$ ) 2SLAQ LRG LF under the assumption that a given fraction of the SDSS LRGs were formed from a major merger of two equal mass progenitors, i.e., we assume that two 2SLAQ LRGs have merged between  $z = 0.55$  and  $z = 0.2$  to form a more massive SDSS LRG. We then

determine the likely fraction of  $z = 0.2$  LRGs that could have been formed this way by fitting (via  $\chi^2$ ) this model to the observed  $z = 0.55$  2SLAQ LRG luminosity function. We could have performed this test using the actual data, rather than fitting the  $z = 0.2$  SDSS LRG LF, but unfortunately such a method would suffer from small number statistics at the bright end of the LF, resulting in the brightest bin disappearing as there are no brighter LRGs being split to refill the bin. However, the  $\chi^2$  values are almost identical for the other bins.

The results are presented in Figure 10 and listed in Table 5. They reveal that the 2SLAQ and SDSS LFs are consistent with each other without any need for merging. At the  $3\sigma$  level, we can exclude merger rates of  $> 50\%$ , i.e., more than half the LRGs at  $z = 0.2$  are already well-assembled, with more than half their stellar mass in place, by  $z \simeq 0.6$ . This observation is consistent with Masjedi et al. (2005) who find that LRG-LRG mergers can not be responsible for the mass growth of LRGs at  $z < 0.36$  based on the small-scale clustering amplitude of SDSS LRG correlation function.

Our limit is barely consistent with the predictions in Figure 5 of De Lucia et al. (2005), where they show that  $\sim 50\%$  of  $z = 0$  massive ellipticals have accreted 50% of their stellar mass since  $z \simeq 0.8$ . We note that our simple model does not constrain the rate of minor mergers; the results of Roseboom et al. (2006) on the spectral analysis of 2SLAQ LRGs suggests the  $\simeq 1\%$  of our LRGs have experienced a small burst of star-formation in the last Gigayear (based on the observed H $\delta$  line), which affects less than 10% of their stellar mass.

Our results are a challenge for models of hierarchical galaxy formation. More detailed comparisons with semi-analytical CDM models are required and will be investigated in other papers. For example, Bower et al. (2005) also include AGN feedback in their semi-analytic simulations, but follow the model suggested by Binney (2004) whereby the AGN heating and the gas cooling form a self-regulating feedback loop if the gas is in the hydrostatic cooling regime (found in groups and cluster) and the central black hole is suitably massive. Initial results suggest that the Bower et al. (2005) prescription provides a better fit to the LRG evolution discussed here (Bower, priv. comm.). We also have significantly more data than used in this paper, i.e., if we could precisely model the K+e corrections of these LRGs over the joint redshift range of the SDSS & 2SLAQ surveys, we would gain a factor of 2 increase in the number of LRGs used to compute their luminosity functions. In future work, we will investigate the use of other stellar synthesis models for such corrections (Maraston 2005).

## ACKNOWLEDGEMENTS

The authors are very grateful to Carlton Baugh, Richard Bower, Darren Croton, Yeong Loh, Claudia Maraston, Daniel Thomas, and Russell Smith for advice and comments on this work. The authors thank the AAO staff for their assistance during the collection of these data. We are also grateful to PPARC TAC and ATAC for their generous allocation of telescope time to this project. DAW thanks the ICG Portsmouth for their financial support during this work. RCN acknowledges the EU Marie Curie program for their

support. IRS and ACE acknowledge support from the Royal Society.

Funding for the SDSS and SDSS-II has been provided by the Alfred P. Sloan Foundation, the Participating Institutions, the National Science Foundation, the U.S. Department of Energy, the National Aeronautics and Space Administration, the Japanese Monbukagakusho, the Max Planck Society, and the Higher Education Funding Council for England. The SDSS Web Site is <http://www.sdss.org/>.

The SDSS is managed by the Astrophysical Research Consortium for the Participating Institutions. The Participating Institutions are the American Museum of Natural History, Astrophysical Institute Potsdam, University of Basel, Cambridge University, Case Western Reserve University, University of Chicago, Drexel University, Fermilab, the Institute for Advanced Study, the Japan Participation Group, Johns Hopkins University, the Joint Institute for Nuclear Astrophysics, the Kavli Institute for Particle Astrophysics and Cosmology, the Korean Scientist Group, the Chinese Academy of Sciences (LAMOST), Los Alamos National Laboratory, the Max-Planck-Institute for Astronomy (MPIA), the Max-Planck-Institute for Astrophysics (MPA), New Mexico State University, Ohio State University, University of Pittsburgh, University of Portsmouth, Princeton University, the United States Naval Observatory, and the University of Washington.

## REFERENCES

- Adelman-McCarthy, J. K., et al. 2005, astro-ph/0507711
- Baldry, I. K., Glazebrook, K., Brinkmann, J., Ivezić, Ž., Lupton, R. H., Nichol, R. C., & Szalay, A. S. 2004, ApJ, 600, 681
- Baldry, I. K., et al. 2005, MNRAS, 358, 441
- Balogh, M. L., Miller, C., Nichol, R., Zabludoff, A., & Goto, T. 2005, MNRAS, 360, 587
- Baugh, C. M., Lacey, C. G., Frenk, C. S., Granato, G. L., Silva, L., Bressan, A., Benson, A. J., & Cole, S. 2005, MNRAS, 356, 1191
- Bell, E. F., et al. 2004, ApJ, 608, 752
- Bell, E. F., et al. 2005, ApJ, 625, 23
- Benson, A. J., Bower, R. G., Frenk, C. S., Lacey, C. G., Baugh, C. M., & Cole, S. 2003, ApJ, 599, 38
- Bernardi, M., Renzini, A., da Costa, L. N., Wegner, G., Alonso, M. V., Pellegrini, P. S., Rit  , C., & Willmer, C. N. A. 1998, ApJL, 508, L143
- Bernardi, M., et al. 2003a, AJ, 125, 1817
- Bernardi, M., et al. 2003b, AJ, 125, 1849
- Bernardi, M., et al. 2003c, AJ, 125, 1866
- Bernardi, M., et al. 2003d, AJ, 125, 1882
- Bernardi, M., Nichol, R. C., Sheth, R. K., Miller, C. J., & Brinkmann, J. 2006, AJ, 131, 1288
- Binney, J. 2004, MNRAS, 347, 1093
- Blanton, M. R., et al. 2003, ApJ, 592, 819
- Bower, R. G., Lucey, J. R., & Ellis, R. S. 1992, MNRAS, 254, 601
- Bower, R., et al. 2005, astro-ph/0511338
- Brough, S., Collins, C. A., Burke, D. J., Mann, R. G., & Lynam, P. D. 2002, MNRAS, 329, L53
- Bruzual, G., & Charlot, S. 2003, MNRAS, 344, 1000
- Cannon, R., et al. 2006, submitted

- Clemens, M. S., Bressan, A., Nikolic, B., Alexander, P., Annibali, F., & Rampazzo, R. 2006, ArXiv Astrophysics e-prints, arXiv:astro-ph/0603714
- Caldwell, N., Rose, J. A., & Concannon, K. D. 2003, AJ, 125, 2891
- Cimatti, A., et al. 2004, Nature, 430, 184
- Collister, A., et al. 2006, MNRAS, submitted
- Croton, D. J., et al. 2006, MNRAS, 365, 11
- De Lucia, G., et al. 2005, astro-ph/0509725
- De Propris, R., Stanford, S. A., Eisenhardt, P. R., Dickinson, M., & Elston, R. 1999, AJ, 118, 719
- Eisenstein, D. J., et al. 2001, AJ, 122, 2267
- Ellis, R. S., Smail, I., Dressler, A., Couch, W. J., Oemler, A. J., Butcher, H., & Sharples, R. M. 1997, ApJ, 483, 582
- Faber, S., et al. 2005, astro-ph/0506044
- Ferrarese, L., & Merritt, D. 2000, ApJL, 539, L9
- Ferreras, I., Lisker, T., Carollo, C. M., Lilly, S. J., & Mobasher, B. 2005, ApJ, 635, 243
- Fioc, M., & Rocca-Volmerange, B. 1997, AA, 326, 950
- Fukugita, M., Ichikawa, T., Gunn, J. E., Doi, M., Shimasaku, K., & Schneider, D. P. 1996, AJ, 111, 1748
- Fukugita, M., Nakamura, O., Turner, E. L., Helmboldt, J., & Nichol, R. C. 2004, ApJL, 601, L127
- Glazebrook, K., et al. 2004, Nature, 430, 181
- Goto, T., et al. 2003, PASJ, 55, 771
- Hogg, D. W., et al. 2002, AJ, 124, 646
- Holden, B. P., et al. 2005, ApJL, 620, L83
- Hopkins, P. F., et al., astro-ph/0508167
- Kauffmann, G. 1996, MNRAS, 281, 487
- Kauffmann, G., et al. 2003, MNRAS, 341, 54
- Kawata, D., & Gibson, B. K. 2005, MNRAS, 358, L16
- Kodama, T., Arimoto, N., Barger, A. J., & Arag'ón-Salamanca, A. 1998, AA, 334, 99
- Kodama, T., et al. 2004, MNRAS, 350, 1005
- Kuntschner, H., & Davies, R. L. 1998, MNRAS, 295, L29
- Kuntschner, H., Smith, R. J., Colless, M., Davies, R. L., Kaldare, R., & Vazdekis, A. 2002, MNRAS, 337, 172
- Le Borgne, D., et al. 2005, ApJ, astro-ph/0503401
- Lilly, S. J., Tresse, L., Hammer, F., Crampton, D., & Le Fevre, O. 1995, ApJ, 455, 108
- Lin, H., Yee, H. K. C., Carlberg, R. G., Morris, S. L., Sawicki, M., Patton, D. R., Wirth, G., & Shepherd, C. W. 1999, ApJ, 518, 533
- McCarthy, P. J., et al. 2004, ApJL, 614, L9
- Maraston, C. 2005, MNRAS, 362, 799
- Masjedi, M., et al., 2005, astro-ph/0512166
- Metcalfe, N., et al., 1996, Nature, 383, 236
- Metcalfe, N., et al., 2001, MNRAS, 323, 795
- Metcalfe, N., et al., 2005, MNRAS, submitted (astro-ph/0509540)
- Naab, T., et al. 2005, astro-ph/0512235
- Nelan, J. E., Smith, R. J., Hudson, M. J., Wegner, G. A., Lucey, J. R., Moore, S. A. W., Quinney, S. J., & Suntzeff, N. B. 2005, ApJ, 632, 137
- Novak, G. S., Faber, S. M., & Dekel, A. 2006, ApJ, 637, 96
- Padmanabhan, N., et al. 2005, MNRAS, 359, 237
- Papovich, C., Dickinson, M., Giavalisco, M., Conselice, C. J., & Ferguson, H. C. 2005, ApJ, 631, 101
- Pimblet, K. A., Smail, I., Edge, A. C., O'Hely, E., Couch, W. J., & Zabludoff, A. I. 2006, MNRAS, 366, 645
- Pozzetti, L., et al. 2003, A&A, 402, 837
- Roseboom, I., et al. 2005, in prep.
- Scannapieco, E., Silk, J., & Bouwens, R. 2005, ApJL, 635, L13
- Schade, D., et al. 1999, ApJ, 525, 31
- Schlegel, D. J., Finkbeiner, D. P., & Davis, M. 1998, ApJ, 500, 525
- Scranton, R., et al. 2005, astro-ph/0508564
- Springel, V., Di Matteo, T., & Hernquist, L. 2005, ApJL, 620, L79
- Strauss, M. A., et al. 2002, AJ, 124, 1810
- Trager, S. C., Faber, S. M., Worthey, G., & González, J. J. 2000, AJ, 120, 165
- Tremaine, S., et al. 2002, ApJ, 574, 740
- Thomas, D., Maraston, C., Bender, R., & de Oliveira, C. M. 2005, ApJ, 621, 673
- van Dokkum, P. G., & Franx, M. 1996, MNRAS, 281, 985
- van Dokkum, P. G., Franx, M., Fabricant, D., Illingworth, G. D., & Kelson, D. D. 2000, ApJ, 541, 95
- Van Dokkum, P. G. 2005, AJ, 130, 2647
- Wake, D. A., Collins, C. A., Nichol, R. C., Jones, L. R., & Burke, D. J. 2005, ApJ, 627, 186
- Yamada, T., et al. 2005, ApJ, 634, 861
- York, D. G., et al. 2000, AJ, 120, 1579

## APPENDIX A: K AND EVOLUTIONARY CORRECTIONS

We present here tables of the  $g - i$  colours, K and K+e corrections derived from the Bruzual & Charlot (2003) models described in Section 3.1.



**Table A1.** K and K+e corrections for the SDSS LRGs to  $z = 0.2$  assuming the passive model discussed in the text

$z$	K					K+e			
	$g-i$	$u$	$g$	$r$	$i$	$u$	$g$	$r$	$i$
0.150	1.697	-0.398	-0.280	-0.086	-0.035	-0.312	-0.214	-0.030	0.017
0.175	1.813	-0.207	-0.141	-0.043	-0.018	-0.162	-0.108	-0.015	0.008
0.200	1.929	0.000	0.000	0.000	0.000	0.000	0.000	0.000	0.000
0.225	2.034	0.202	0.132	0.042	0.017	0.159	0.098	0.015	-0.008
0.250	2.121	0.422	0.254	0.088	0.043	0.336	0.185	0.032	-0.008
0.275	2.208	0.647	0.376	0.140	0.069	0.523	0.272	0.056	-0.007
0.300	2.300	0.879	0.506	0.190	0.097	0.726	0.367	0.079	-0.005
0.325	2.393	1.116	0.644	0.242	0.128	0.934	0.466	0.104	0.001
0.350	2.450	1.333	0.753	0.303	0.168	1.125	0.537	0.137	0.015

**Table A2.** K and K+e corrections for SDSS LRGs to  $z = 0.2$  assuming the passive plus star-forming model discussed in the text

$z$	K					K+e			
	$g-i$	$u$	$g$	$r$	$i$	$u$	$g$	$r$	$i$
0.150	1.597	-0.217	-0.244	-0.078	-0.032	-0.189	-0.195	-0.029	0.016
0.175	1.703	-0.107	-0.123	-0.039	-0.016	-0.095	-0.098	-0.014	0.007
0.200	1.808	0.000	0.000	0.000	0.000	0.000	0.000	0.000	0.000
0.225	1.903	0.094	0.113	0.038	0.016	0.086	0.088	0.014	-0.007
0.250	1.982	0.186	0.217	0.079	0.039	0.174	0.167	0.030	-0.007
0.275	2.060	0.268	0.321	0.126	0.064	0.261	0.246	0.053	-0.006
0.300	2.143	0.340	0.429	0.170	0.089	0.343	0.332	0.074	-0.003
0.325	2.225	0.402	0.542	0.217	0.118	0.417	0.420	0.097	0.003
0.350	2.275	0.444	0.631	0.271	0.155	0.472	0.484	0.128	0.017

**Table A3.** K and K+e corrections for 2SLAQ LRGs to  $z = 0.55$  assuming the passive model discussed in the text

$z$	K					K+e			
	$g-i$	$g$	$r$	$i$	$z$	$g$	$r$	$i$	$z$
0.450	2.574	-0.402	-0.470	-0.140	-0.086	-0.256	-0.328	-0.042	0.000
0.475	2.635	-0.298	-0.351	-0.111	-0.066	-0.190	-0.244	-0.037	-0.001
0.500	2.682	-0.204	-0.227	-0.075	-0.049	-0.131	-0.157	-0.025	-0.006
0.525	2.735	-0.105	-0.110	-0.041	-0.027	-0.069	-0.074	-0.016	-0.005
0.550	2.788	0.000	0.000	0.000	0.000	0.000	0.000	0.000	0.000
0.575	2.850	0.115	0.103	0.040	0.027	0.078	0.068	0.016	0.005
0.600	2.921	0.245	0.203	0.084	0.058	0.169	0.136	0.036	0.014
0.625	3.001	0.394	0.306	0.137	0.093	0.278	0.208	0.064	0.027
0.650	3.077	0.546	0.414	0.200	0.126	0.389	0.284	0.101	0.037

**Table A4.** K and K+e corrections for 2SLAQ LRGs to  $z = 0.55$  assuming the passive plus star-forming model discussed in the text.

$z$	K					K+e			
	$g-i$	$g$	$r$	$i$	$z$	$g$	$r$	$i$	$z$
0.450	2.376	-0.244	-0.412	-0.126	-0.080	-0.189	-0.308	-0.039	-0.001
0.475	2.422	-0.177	-0.308	-0.100	-0.061	-0.139	-0.230	-0.035	-0.002
0.500	2.455	-0.118	-0.199	-0.067	-0.045	-0.095	-0.148	-0.024	-0.006
0.525	2.491	-0.060	-0.096	-0.037	-0.025	-0.049	-0.070	-0.015	-0.005
0.550	2.526	0.000	0.000	0.000	0.000	0.000	0.000	0.000	0.000
0.575	2.566	0.063	0.090	0.036	0.025	0.055	0.065	0.015	0.005
0.600	2.609	0.130	0.177	0.076	0.053	0.118	0.129	0.034	0.014
0.625	2.655	0.202	0.268	0.123	0.086	0.191	0.198	0.061	0.026
0.650	2.693	0.269	0.361	0.178	0.117	0.263	0.270	0.095	0.036

**Table A5.** K and K+e corrections for SDSS LRGs to  $z = 0.55$ 

z	g − i	u → g	Passive					g − i	u → g	Star-forming					g − i	u → g
			K			K+e				K			K+e			
			g → r	r → i	u → g	g → r	r → i			g → r	r → i	u → g	g → r	r → i		
0.150	1.697	0.200	0.031	-0.012	0.727	0.501	0.386	1.597	0.381	0.067	-0.004	0.850	0.520	0.387		
0.175	1.813	0.391	0.170	0.031	0.877	0.607	0.401	1.703	0.491	0.188	0.035	0.944	0.617	0.402		
0.200	1.929	0.598	0.311	0.074	1.039	0.715	0.416	1.808	0.598	0.311	0.074	1.039	0.715	0.416		
0.225	2.034	0.800	0.443	0.116	1.198	0.813	0.431	1.903	0.703	0.434	0.118	1.113	0.802	0.429		
0.250	2.121	1.020	0.565	0.162	1.375	0.900	0.448	1.982	0.830	0.573	0.176	1.159	0.876	0.441		
0.275	2.208	1.245	0.687	0.214	1.562	0.987	0.472	2.060	0.920	0.685	0.227	1.237	0.954	0.463		
0.300	2.300	1.477	0.817	0.264	1.765	1.082	0.495	2.143	0.992	0.793	0.271	1.319	1.040	0.484		
0.325	2.393	1.714	0.955	0.316	1.973	1.181	0.520	2.225	1.054	0.906	0.318	1.393	1.128	0.507		
0.350	2.450	1.931	1.064	0.377	2.164	1.252	0.553	2.275	1.096	0.995	0.372	1.448	1.192	0.538		

**Table A6.** K and K+e corrections for 2SLAQ LRGs to  $z = 0.2$ 

Passive										Star-forming					
			K			K+e			K			K+e			
z	$g-i$	$r \rightarrow g$	$i \rightarrow r$	$z \rightarrow i$	$r \rightarrow g$	$i \rightarrow r$	$z \rightarrow i$	$g-i$	$r \rightarrow g$	$i \rightarrow r$	$z \rightarrow i$	$r \rightarrow g$	$i \rightarrow r$	$z \rightarrow i$	
0.450	2.574	-0.781	-0.214	-0.183	-1.043	-0.458	-0.408	2.376	-0.776	-0.227	-0.192	-1.016	-0.449	-0.402	
0.475	2.635	-0.662	-0.185	-0.163	-0.959	-0.453	-0.409	2.422	-0.672	-0.201	-0.173	-0.938	-0.445	-0.403	
0.500	2.682	-0.538	-0.149	-0.146	-0.872	-0.441	-0.414	2.455	-0.563	-0.168	-0.157	-0.856	-0.434	-0.407	
0.525	2.735	-0.421	-0.115	-0.124	-0.789	-0.432	-0.413	2.491	-0.460	-0.138	-0.137	-0.778	-0.425	-0.406	
0.550	2.788	-0.311	-0.074	-0.097	-0.715	-0.416	-0.408	2.526	-0.364	-0.101	-0.112	-0.708	-0.410	-0.401	
0.575	2.850	-0.208	-0.034	-0.070	-0.647	-0.400	-0.403	2.566	-0.274	-0.065	-0.087	-0.643	-0.395	-0.396	
0.600	2.921	-0.108	0.010	-0.039	-0.579	-0.380	-0.394	2.609	-0.187	-0.025	-0.059	-0.579	-0.376	-0.387	
0.625	3.001	-0.005	0.063	-0.004	-0.507	-0.352	-0.381	2.655	-0.096	0.022	-0.026	-0.510	-0.349	-0.375	
0.650	3.077	0.103	0.126	0.029	-0.431	-0.315	-0.371	2.693	-0.003	0.077	0.005	-0.438	-0.315	-0.365	